Chinese Journal of
POLYMER SCIENCE

ARTICLE

https://doi.org/10.1007/s10118-019-2206-3
Chinese J. Polym. Sci. **2019**, *37*, 401–408

NIR Emission Nanoparticles Based on FRET Composed of AIE Luminogens and NIR Dyes for Two-photon Fluorescence Imaging

Lei-Jing Liu[a†], Wen Liu[b†], Guang Ji[a], Zhi-Yuan Wu[a], Bin Xu[a], Jun Qian[b*], and Wen-Jing Tian[a*]

[a] *State Key Lab for Supramolecular Structure and Materials, Jilin University, Changchun 130012, China*
[b] *State Key Laboratory of Modern Optical Instrumentations, Centre for Optical and Electromagnetic Research, JORCEP (Sino-Swedish Joint Research Center of Photonics), Zhejiang University, Hangzhou 310058, China*

Abstract Near-infrared (NIR) nanoparticles (NPs) based on fluorescence resonance energy transfer (FRET) were prepared by co-encapsulation of a red aggregation-induced emission (AIE) molecule, 2-(4-bromophenyl)-3-(4-(4-(diphenylamino)styryl)phenyl)fumaronitrile (TB), and a commercial NIR fluorescence dye, silicon 2,3-naphthalocyanine bis(trihexylsilyloxide) (NIR775) with an amphiphilic polymer poly(styrene-*co*-maleic anhydride) (PSMA). The surface of the NPs, PSMA@TB/NIR775, was modified with poly(ethylene glycol) (PEG) to increase the *in vivo* biocompatibility of the NPs. The PSMA@TB/NIR775 NPs showed a strong NIR (780 nm) narrow emission and excellent two-photon absorption property. Moreover, the NPs exhibited good monodispersity, stability, and low cytotoxicity. Under the excitation of a 1040 nm femtosecond (fs) laser, the emission peaks at 680 nm of TB and 780 nm of NIR775 excited by FRET were obtained. We utilized PSMA@TB/NIR775 NPs as fluorescent contrast agents for two-photon excited NIR microscopic imaging, and good NIR imaging effect of mouse brain vasculature was obtained with the imaging depth of about 150 μm. The FRET strategy by co-encapsulating AIE molecule and NIR dye will be helpful in preparing more narrow emission NIR probes for deep-tissue biological imaging.

Keywords NIR emission; AIE; FRET; Two-photon imaging; Amphiphilic polymer

Citation: Liu, L. J.; Liu, W.; Ji, G.; Wu, Z. Y.; Xu, B.; Qian, J.; Tian, W. J. NIR emission nanoparticles based on FRET composed of AIE luminogens and NIR dyes for two-photon fluorescence imaging. *Chinese J. Polym. Sci.* **2019**, *37*, 401–408.

INTRODUCTION

Polymer-encapsulated nanoparticles (NPs) have attracted much attention in the application of bioimaging and bioassay because of the optical transparence and biological compatibility of polymers as encapsulation matrixes. Furthermore, the encapsulation can protect dye molecules from the external perturbation.[1−3]

The fluorescence probe with near-infrared (NIR) light (700−900 nm) emission is very important in the field of cancer diagnosis and treatment due to its advantages of low optical damage, deep tissue penetration depth, and minimal effect of biological tissue autofluorescence. So far, the most widely investigated NIR fluorescent probes are inorganic quantum dots (QDs) and organic fluorescent dyes.[4−6] However, inorganic QDs can release heavy metal ions in oxidative environment and exhibit high toxicity, which limits their applications.[7−10] As for organic fluorescent dyes, the traditional organic dyes are usually excited by visible light with a small Stokes shift, and suffer from poor optical stability and photobleaching.[11−15] In addition, the fluorescence intensity of the traditional organic dye will decrease when it aggregates into nanoparticles at high concentrations due to the strong hydrophobic interaction and π-π stacking interaction,[16,17] known as aggregation-caused quenching (ACQ) effect.[18] Therefore, the development of organic fluorescent probes with NIR emission, low toxicity, large Stokes shift, good photostability, high brightness, and anti-photobleaching is still a big challenge.

Fortunately, Tang *et al*. developed a novel class of fluorogens with aggregation-induced emission (AIE) features.[19−21] Unlike ACQ dyes, the emission of AIE luminogens (AIEgens) will be enhanced rather than quenched in response to aggregation. Moreover, AIEgens exhibit some merits such as high photobleaching threshold, stable fluorescence, and low cytotoxicity.[22−25] These benefits make AIEgens ideal probes for bioimaging.[26−29] Recently, many AIE fluorescent molecules with red/NIR emission have been designed and synthesized.[1−3,30−35] However, these molecules have such undesirable qualities as one or another when used in the bioimaging. For example, some of their emission maxima were mainly located at wavelengths shorter than 650 nm and only part of their emission spectra was located in the NIR range.[30−33] Some of these AIE fluorescent molecules showed broad emission spectra.[3,34] The wide emission spectra would interfere with the detection of other synchronous

* Corresponding authors: E-mail qianjun@zju.edu.cn (J.Q.)
E-mail wjtian@jlu.edu.cn (W.J.T.)
† These authors contributed equally to this work.
Invited article for special issue of "AIE-active Polymer"
Received October 24, 2018; Accepted December 9, 2018; Published online January 10, 2019

signals, which limits the application of the fluorescent probes. Thus, the development of AIE fluorescent probes with narrow NIR emission is of great significance, while a simple single molecule design is difficult to achieve such a goal.

Fluorescence resonance energy transfer (FRET) occurs between two molecules, donor and acceptor, when they are close enough. FRET needs to meet the condition that the emission spectrum of donor overlaps with the absorption spectrum of the acceptor, and the distance between the donor molecule and the acceptor molecule is less than 100 nm. In FRET process, the excitation luminescence first excites the donor to its electronic excited state. Then, the energy transfers from donor to acceptor, and the acceptor is excited to its electronic excited state. Finally, the acceptor falls back to its ground state, and resultantly the emitted photons are mostly from the acceptor, leading to large apparent Stokes shifts.[36−42] Compared with the complex molecular designing, FRET strategy can more readily achieve the fluorescence probe of NIR emission with high efficiency. Encapsulation of a suitable traditional commercial NIR dye together with an AIE molecule to achieve FRET nanoparticles can not only obtain the narrow NIR emission, but also prevent the fluorescence quenching, resulting in strong NIR fluorescence and good photostability of NPs.[30−33,43]

The two-photon fluorescence microscopy (TPFM) imaging technique is a deep tissue imaging method. The excitation source is a femtosecond (fs) laser, and the excitation wavelength in most TPFM is located within 700−900 nm,[44] which is beneficial to increasing the penetration depth of excitation light. In addition, due to the nonlinear excitation mode of the two-photon fluorescence, only the local particles where the light beam focuses can be excited, and other regions of the biological samples without the light beam will not be excited, which largely prevents the photobleaching of fluorescent probes and increases the spatial resolution of the imaging.[45−50]

In this work, a red emissive AIE molecule, 2-(4-bromophenyl)-3-(4-(4-(diphenylamino)styryl)phenyl)fumaronitrile (TB), was chosen as the FRET donor, and silicon 2,3-naphthalocyanine bis(trihexylsilyloxide) (NIR775), a commercial NIR dye, was selected as the acceptor. FRET pairs of different ratios were co-encapsulated[42,51,52] into the amphiphilic polymer poly(styrene-*co*-maleic anhydride) (PSMA) to prepare the NIR FRET NPs of PSMA@TB/NIR775. The results indicated that the NPs have strong NIR (780 nm) luminescence, good two-photon properties, excellent monodispersity, stability, and low cytotoxicity. We used 1040 nm femtosecond (fs) laser as the excitation source to excite the NPs,[53] and the emission peaks located at 680 nm of TB and 780 nm of NIR 775 excited by FRET were obtained. The two-photon imaging of mice brain vasculature measured with the NPs had a good NIR imaging effect, and the imaging depth was about 150 μm.

EXPERIMENTAL

Materials

All reagents and starting materials were commercially available and were used without further purification. The detailed synthesis and characterization of TB have been reported in our previous work.[54] Tetrahydrofuran (THF) was bought from Xilong Chemical Co., Ltd. 1-(3-Dimethylaminopropyl)-3-ethylcarbodiimide hydrochloride (EDC) was purchased from Sam Chemical Technology (Shanghai) Co., Ltd. *N*-hydroxysuccinimide (NHS) was obtained from Sinopharm Chemical Reagent Co., Ltd. PEG-NH_2, PSMA, 3-(4,5-dimethyl-2-thiazolyl)-2,5-diphenyl-2-*H*-tetrazolium bromide, and thiazolyl blue tetrazolium bromide (MTT) were bought from Sigma-Aldrich (St. Louis, MO, USA). Dulbecco's modified eagle medium (DMEM) cell culture medium was purchased from Hyclone Corporation. All other chemicals were purchased as analytical grade from Sinopharm Chemical Reagent Co., Ltd. Deionized water (18.2 MΩ·cm resistivity) from a Milli-Q water system was used throughout the whole experiments.

Experimental Instrument

UV-Vis absorption spectra were recorded on a Shimadzu UV-3600 spectrophotometer. Fluorescence spectra were recorded on an Ocean Optics Maya2000Pro optical fiber spectrophotometer with a 405 nm LED as the excitation source. DLS and zeta potential measurements were performed using a Malvern Zetasizer Nano ZS size analyzer at room temperature. The morphology of NPs was characterized by a field emission transmission electron microscope (FE-TEM, JEM-2100F, JEOL, Japan). Two-photon fluorescence spectra of PSMA@TB/NIR775 NPs, which were excited by a 1040 nm fs laser (from an amplified output of a large-mode-area ytterbium-doped photonic crystal fiber (PCF) oscillator (150 fs, 50 MHz)), were measured by a home-built system and collected with an optical fiber spectrometer (PG2000, Ideaoptics Instruments).

Preparation and Surface Modification of Nanoparticles

PSMA@TB/NIR775 NPs nanoparticles were prepared by using a self-assembly method. TB stock solution of THF (1 mg/mL, 5 mL), PSMA stock solution of THF (5 mg/mL, 20 mL), and NIR775 stock solution of THF (0.1 mg/mL, 10 mL) were prepared, respectively. Then 100 μL of TB stock solution and 200 μL of PSMA stock solution were mixed in a 2 mL-EP tube, and different amounts of NIR775 stock solutions (20, 30, 40, 50, 60, 70, 80, and 90 μL), respectively, were added. THF (1 mL) was added to the solutions under ultrasonication. The doping ratios of NIR775 were 2%−9% when taking TB as the reference. Deionized water (5 mL) was added into a 20 mL-glass bottle and placed in an ultrasonic instrument at about 40 °C, and the solutions in EP tubes were quickly poured into the bottle after the water was heated under ultrasonication. The solutions were heated on a hot stage at 78 °C 5 min later, and nitrogen was blown into the solutions to remove the THF until there was no smell in the bottle (It was suitable that the bubbles came out continuously and uniformly.). The red NPs were obtained by filtration with 0.22 μm water phase filter.

The aqueous solution of NPs prepared was concentrated by heating in water bath to calculate the encapsulation concentration. The concentrated solution was put into a beaker and heated by ultrasonication with the addition of EDC.

https://doi.org/10.1007/s10118-019-2206-3

After 10 min of ultrasonication, NHS was added into the beaker and the solution was activated for 5 min. Then PEG-NH_2 was added to the mixed solution, and the solution reacted under ultrasonication for 2 h. Finally, the mixture was removed to the semipermeable membrane by a syringe, and dialyzed in the $NaHCO_3$ solution for 12 h. Dialysate changed to deionized water, the solution was dialyzed for 3 days with the deionized water renovated once every 6 h until the NP solution was clear and transparent. The PEG-modified NPs were obtained after the NP solution was filtered by 0.22 μm water phase filter.

Cytotoxicity of NPs

The cytotoxicity of NPs on HepG2 cells was evaluated by an MTT assay. Cell viability was used to evaluate the cytotoxicity of the NPs. HepG2 cells in normal division and growth were laid in a 96-well plate at the concentration of 1×10^5 cells/mL, and each well contained 100 μL of the sample. The plate was placed in an incubator with 5% carbon dioxide and incubated at 37 °C for 24 h. After removing the original culture medium, DMEM (containing 2% serum) fresh medium containing different concentrations of NPs (0, 20, 40, 60, 80, 100, and 120 μg/mL) was added to each well. Then the plate was placed in the incubator with 5% carbon dioxide and incubated at 37 °C for 24 h, followed by addition of MTT solution (5 mg/mL, 10 μL), and incubation for another 4 h. The samples without NPs acted as the positive control group. After removing the supernatant of the wells, 200 μL of DMSO was added and vibrated at room temperature for 5 min. The absorbance at 650 nm was detected by using a microplate reader after the crystals were dissolved completely.

Two-photon Fluorescence Imaging

All animal experiments were conducted under the requirements and guidelines of the Experimental Animal Ethics Committee of Zhejiang University. ICR mice (~18 g, female) were obtained from the Animal Center Laboratory of Zhejiang University, and caged in a super-clean room. All the drinking water and food were of experimental level, and their housing area was kept at 24 °C with a 12 h day/night cycle. Initially, the anesthetized mice underwent skull-removal surgery under aseptic conditions to prevent infection and other injuries. ICR mice were intravenously injected with 300 μL of PSMA@TB/NIR775 NPs (0.125 mg/mL in PBS buffer solution). The mice of the control group were intravenously injected with 300 μL of PSMA@NIR775 NPs without TB (PBS buffer solution). The mice were imaged on a two-photon fluorescence scanning microscope under the excitation of a 1040 nm femtosecond (fs) laser (150 fs, 50 MHz). To ensure a normal life activity, the temperature of the mice was maintained at (37 ± 1) °C. The two-photon signals were filtered using a 590 nm long-pass filter, and collected using the photomultiplier tube (PMT, H7422-50, Hamamatsu) through NDD mode.

RESULTS AND DISCUSSION

Preparation and Properties of PSMA@TB/NIR775 NPs

Scheme 1 illustrates the schematic diagram for the preparation of PSMA@TB/NIR775 fluorescent NPs by co-encapsulation of TB and NIR775 with amphiphilic polymer PSMA. The chemical structures of the compounds are shown in the schematic diagram. Under ultrasonication conditions, hydrophilic-hydrophobic interaction acts as the self-assembly dynamics of the NPs. The hydrophobic segments of PSMA intertwine with the dye molecules, TB and NIR775, to form hydrophobic nuclei. The maleic anhydride groups on the polymeric chains hydrolyze to carboxylic acids under ultrasonication conditions. The carboxylic acids as hydrophilic groups distribute evenly on the surface of the hydrophobic nucleus to form a water-soluble shell, ensuring that the NPs are water-soluble and will not aggregate. This enables the NPs to exhibit good monodispersity and long-term stability in aqueous solution. The fluorescent NPs modified with PEG

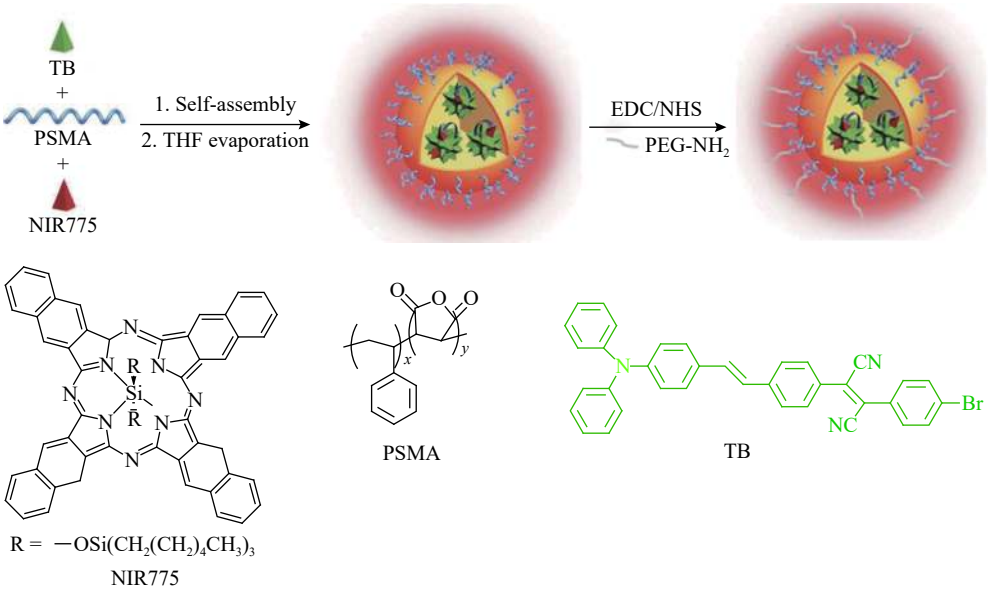

Scheme 1 The chemical structures and synthetic approach of PSMA@TB/NIR775 NPs

https://doi.org/10.1007/s10118-019-2206-3

were prepared through dehydration condensation of carboxylic acid and amino group on the NPs surface.

The size and morphology of the prepared NPs were characterized by dynamic light scattering (DLS) and transmission electron microscopy (TEM). As shown in Fig. 1(a), the PSMA@TB/NIR775 NPs have a relatively uniform particle size distribution, and the average hydrodynamic diameter (number-weighted) of the NPs is 64.5 nm. From the TEM morphology, it can be found that the size distribution of the NPs is also uniform with an average diameter of 40.8 nm, and the particles present a uniform sphere shape (Fig. 1b). The particle size measured by TEM is smaller than that measured by DLS due to the drying process for TEM measurement.

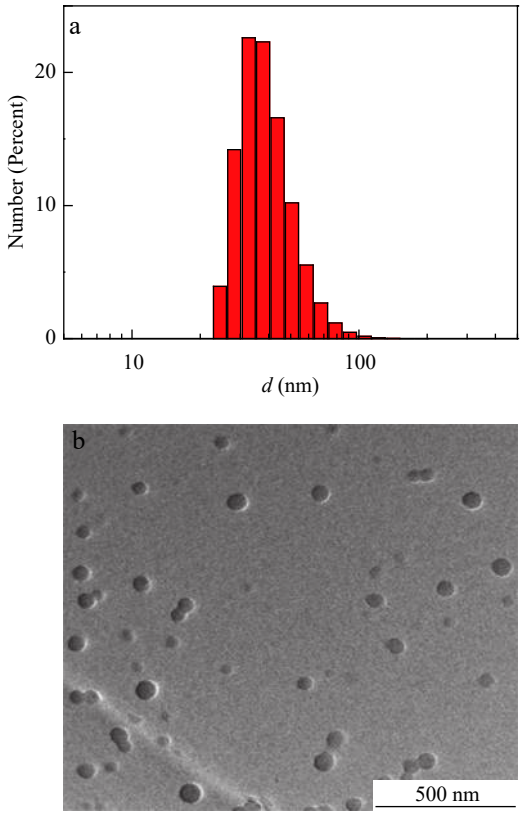

Fig. 1 (a) DLS distribution and (b) TEM morphology of the PSMA@TB/NIR775 NPs

Fig. 2 shows the zeta potential of the PSMA@TB/NIR775 NPs. The surface potential of the NPs is −67.8 mV. The low surface potential results from the large number of carboxyl groups produced by hydrolysis of acid anhydride on the NPs surface, and the ionization of the carboxyl groups causes more negative charges on particle surface. According to the principle of mutual exclusion of the charges with the same sign, the PSMA@TB/NIR775 NPs will not aggregate in a short time. No obvious precipitation was observed after storage of two months at room temperature, indicating that the NPs solution has an excellent colloidal stability. Overall, the prepared fluorescent NPs have good monodispersity, uniform size distribution, and good stability.

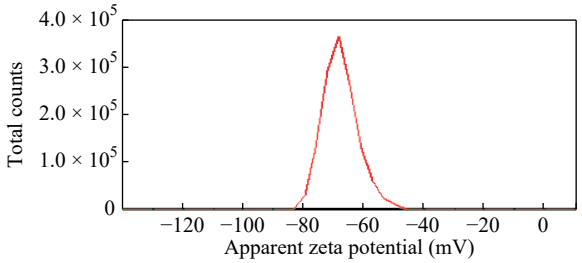

Fig. 2 Zeta potential distribution of the PSMA@TB/NIR775 NPs

Photophysical Properties of PSMA@TB/NIR775 NPs

PSMA@TB NPs were prepared through self-assembly of amphiphilic polymer PSMA and AIE molecule TB under ultrasonication. The normalized absorption and emission spectra of PSMA@TB NPs and NIR775 in THF solution are shown in Fig. 3. PSMA@TB NPs have a strong absorption peak at 357 nm and a weak absorption peak at 475 nm. For the emission spectrum, PSMA@TB NPs show a broad emission peak at 560−866 nm with the maximum located at 678 nm. NIR775 shows three absorption peaks at 688, 733, and 773 nm, and three emission peaks at 790, 818, and 860 nm, respectively. All the absorption and emission peaks of NIR775 exhibit a narrow characteristic. In addition, all the absorption wavelengths of NIR775 fall within the fluorescence emission wavelength range of PSMA@TB NPs. It is well known that FRET can be realized if the absorption spectrum of one molecule overlaps with the emission spectrum of another molecule. Consequently, FRET NPs can be obtained by co-encapsulation of TB and NIR775 with amphiphilic polymer PSMA.

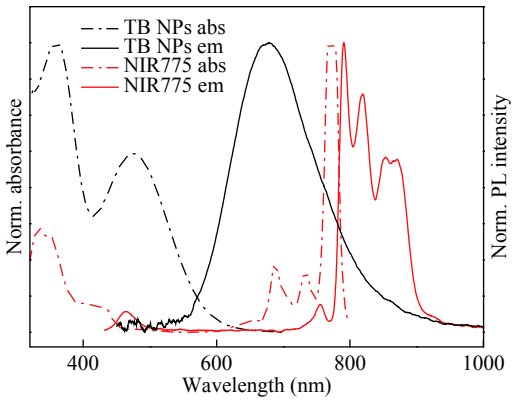

Fig. 3 Normalized absorption and emission spectra (under the excitation of a 405 nm LED) of PSMA@TB NPs and NIR775 in THF solution

To obtain the optimized NIR emission, we investigated the influence of NIR775 feeding ratios on the absorption spectra of PSMA@TB/NIR775 NPs. Herein, the amount of TB and PSMA was fixed, while the mass ratio of NIR775 to TB was varied from 3% to 8%. The absorption spectra of PSMA@TB/NIR775 NPs are shown in Fig. 4(a). It can be found that the absorption intensity of PSMA@TB/NIR775 NPs around 773 nm increases as the mass ratio of NIR775/TB increases from 3% to 8% (with the same amount of TB). Fig. 4(b) illustrates the change in emission spectra

https://doi.org/10.1007/s10118-019-2206-3

with increasing concentrations of NIR775 from 2% to 9%. The TB emission from 600 nm to 750 nm is quenched gradually, and the 780 nm emission of NIR775 increases with the mass ratio changing from 2% to 5%. This is because NIR775 molecules are separated by the AIE molecules TB in the PSMA matrix. TB molecule displays highly twisted molecular conformation, which will weaken the π-π stacking effect with NIR775, so the fluorescence quenching of NIR775 can be avoided.[55,56] When the mass ratio of NIR775 in PSMA@TB/NIR775 NPs is larger than 5%, the emission at 780 nm declines due to the quenching of NIR775 dyes. This is because a higher concentration of NIR775 dyes results in the π-π stacking effect with each other. PSMA@TB/NIR775 NPs with a 5% loading ratio of NIR775 exhibit the strongest fluorescence signals at 780 nm. Thus, PSMA@TB/NIR775 NPs with a 5% loading ratio of NIR775 was adopted to conduct the following cytotoxicity experiments and two-photon imaging experiments.

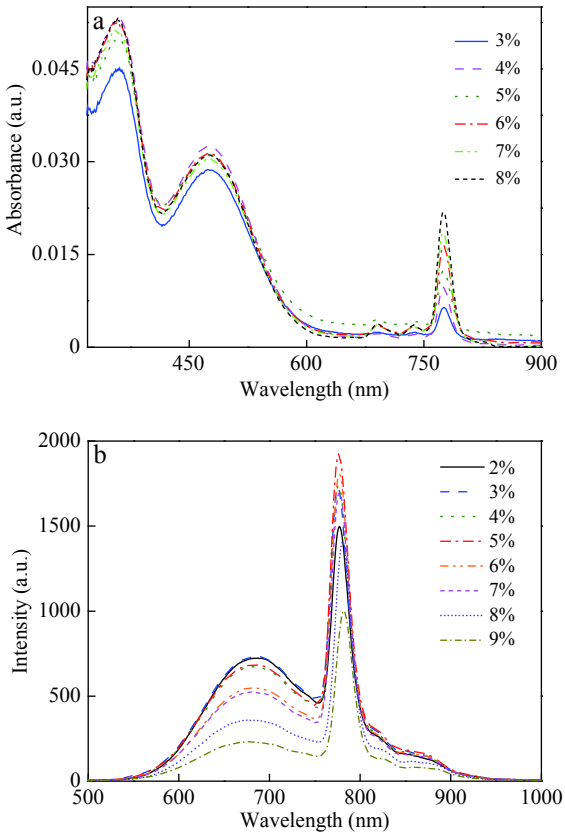

Fig. 4 (a) Absorption spectra and (b) emission spectra (under the excitation of a 405 nm LED) of PSMA@TB/NIR775 NPs with different NIR775 doping concentrations

FRET process between donor and acceptor is usually associated with the lifetime change of donor in the absence and presence of acceptor. Larger lifetime changes indicate more efficient energy transfer between the FRET pair.[57] Fig. 5 shows the fluorescence decay curves of PSMA@TB NPs and FRET NPs (PSMA@TB/NIR775). PSMA@TB NPs without doping NIR775 have an initial lifetime of 3.84 ns, which decreases to 2.63 ns by doping with 5% NIR775. The obvious lifetime difference demonstrates the efficient energy transfer between TB and NIR775. FRET efficiency was calculated to be 31.5% by the equation of $\eta = 1 - \tau_{DA}/\tau_D$, where τ_{DA} and τ_D are the lifetimes of FRET NPs (PSMA@TB/NIR775) and the donor TB, respectively. Although the FRET efficiency is not very high, it well proves that the PSMA@TB/NIR775 NPs have FRET effect. Thus, the fluorescent NPs with NIR and narrow emission were successfully obtained through FRET.

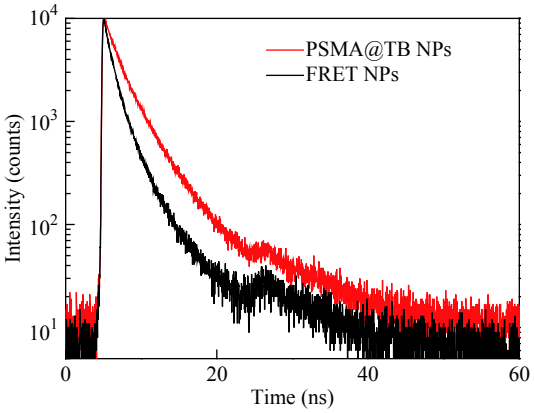

Fig. 5 Fluorescence decay curves of PSMA@TB and FRET NPs PSMA@TB/NIR775 NPs

Cytotoxicity of PSMA@TB/NIR775 NPs

The cytotoxicity of PSMA@TB/NIR775 NPs was assessed with an MTT assay.[58] Fig. 6 shows the cell viability results when incubated with various concentrations (0−120 μg/mL) of PSMA@TB/NIR775 NPs for 24 h. It can be found that the cell viability remains ~90% even when the concentration of PSMA@TB/NIR775 NPs reaches as high as 100 μg/mL, indicating that the NPs prepared have good cytocompatibility, low cytotoxicity, and are suited for biological imaging.

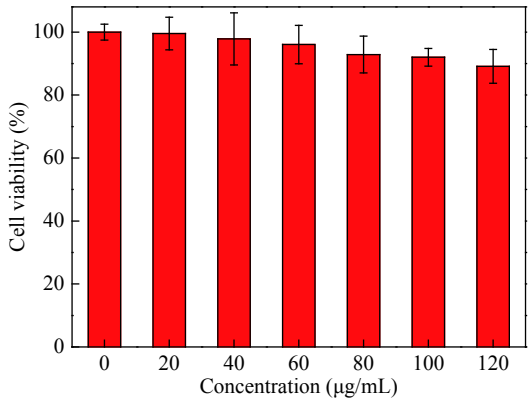

Fig. 6 Viability of HepG2 cells after incubation with different concentrations of PSMA@TB/NIR775 NPs for 24 h. The loading ratio of TB and PSMA is 1:10, and the mass ratio of NIR775 to TB is 5%.

Two-photon Imaging of PSMA@TB/NIR775 NPs

Two kinds of PSMA@TB/NIR775 NPs with 5% and 8% mass ratios of NIR775 to TB were prepared and their two-photo properties were investigated. It is known that TB has

excellent two-photon properties, while NIR775 does not have two-photon absorption. Accordingly, the two-photon absorption cross-section of PSMA@TB/NIR775 should be similar to that of TB. The measurement of two-photon absorption cross-section of TB molecule and the proof of two-photon nonlinear optical process have been reported in our previous studies.[54] Fig. 7 shows the two-photon fluorescence spectra of PSMA@TB/NIR775 NPs by using 1040 nm fs laser (150 fs, 50 MHz) as the exciting light. It can be found that the two-photon spectra are similar to the single-photon spectra of the NPs, indicating that the NPs absorb two photons simultaneously to complete the transition from ground state to excited state. That is, TB emits two-photon fluorescence after absorbing two photons, which further excites the near-infrared dye NIR775 to produce NIR emission of 780 nm. Moreover, the NPs doped with 5% NIR775 have the stronger NIR emission intensity than the NPs doped with 8% NIR775 do, which performs the same as the single photon spectra.

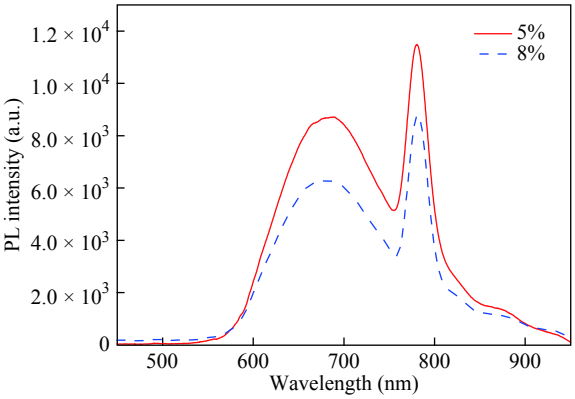

Fig. 7 Two-photon fluorescence spectra of PSMA@TB/NIR775 NPs with 5% and 8% mass ratios of NIR775 to TB (exciting light: 1040 nm fs laser)

Fig. 8 shows the capillary two-photon fluorescence photographs of PSMA@TB/NIR775 NPs with 5% and 8% mass ratios of NIR775, and PSMA@NIR775 NPs without TB. Because PSMA@TB/NIR775 NPs produce two-photon fluorescence, the capillary shape can be clearly seen in Figs. 8(a) and 8(b). The capillary imaging effect of 5% doping ratio is better than that of 8% doping ratio, and the former fluorescence is stronger, which is consistent with the results of the two-photon fluorescence spectra. Since PSMA@NIR775 NPs do not have two-photon absorption, the fluorescence from PSMA@NIR775 NPs does not appear in Fig. 8(c) under the excitation of fs laser.

To demonstrate the potential application of two-photon NIR fluorescence in biological imaging, PSMA@TB/NIR775 NPs with 5% mass ratio of NIR775 were applied to the brain vasculature imaging of a mouse under 1040 nm fs laser excitation. The imaging signals were received at a depth of every 10 μm, and then many fluorescent images with different depths were acquired. Two-photon imaging of the blood vessels was obtained by stacking those fluorescent images along *Z*-axis direction. Fig. 9 shows the two-photon images

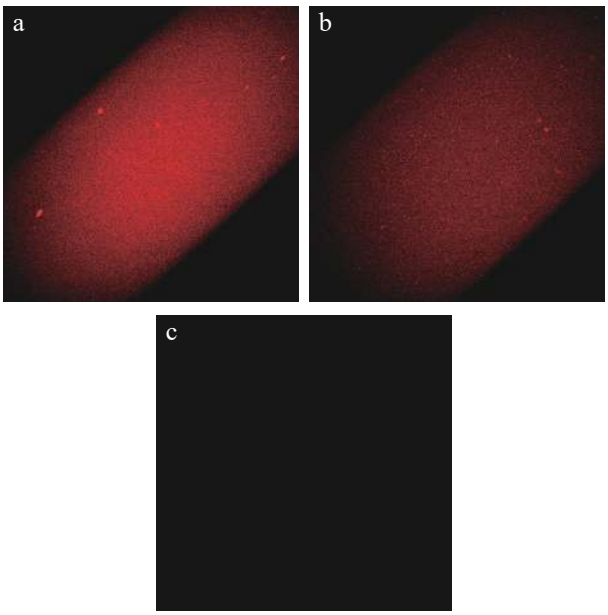

Fig. 8 Capillary two-photon fluorescence photographs of PSMA@TB/NIR775 NPs with (a) 5% and (b) 8% mass ratios of NIR775, and (c) PSMA@NIR775 NPs without TB (exciting light: 1040 nm fs laser)

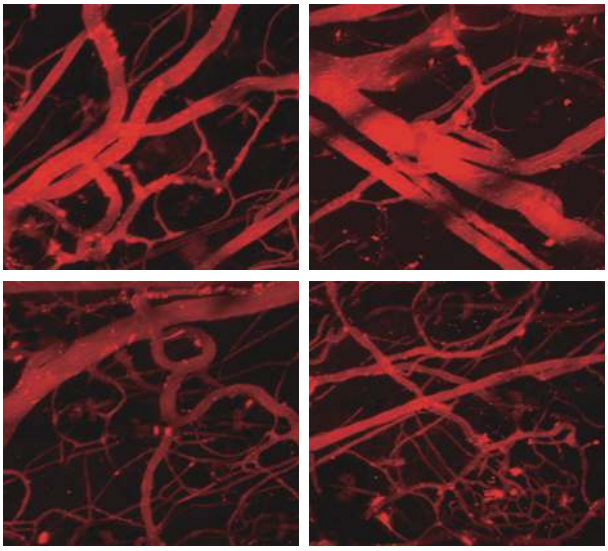

Fig. 9 Two-photon fluorescence imaging of mouse brain vessels in four different places using PSMA@TB/NIR775 NPs

of cerebral vessels at four different areas in a mouse. The depth of the image was about 150 μm. Besides the main veins and arteries, small capillaries in deep places could also be seen. These results indicated that PSMA@TB/NIR775 NPs can be used as angiographic agents for biological vascular imaging *in vivo*.

CONCLUSIONS

In summary, we prepared NIR NPs, PSMA@TB/NIR775, based on FRET by co-encapsulation of a red AIE molecule TB and a commercial NIR fluorescence dye NIR775 with the amphiphilic polymer PSMA. The NPs showed a strong NIR

https://doi.org/10.1007/s10118-019-2206-3

(780 nm) narrow emission peak and excellent two-photon absorption property. Moreover, the NPs exhibited good monodispersity, stability, and low cytotoxicity. The PSMA@TB/NIR775 NPs were excited by using a 1040 nm fs laser as the excitation source, and the emission peaks at 680 nm of TB and 780 nm of NIR775 excited by FRET were obtained. The two-photon NIR imaging of mice brain vasculature using the NPs was achieved, and the imaging depth was about 150 μm. The NIR fluorescent NPs developed in this work can be further conjugated with specific ligands or functional groups for targeted biological imaging or sensing.

ACKNOWLEDGMENTS

This work was financially supported by the National Natural Science Foundation of China (Nos. 21835001, 51773080, 21674041, 51573068, and 21221063), Program for Changbaishan Scholars of Jilin Province, Jilin Province (No. 20160101305JC), and the "Talents Cultivation Program" of Jilin University.

REFERENCES

1 Yan, L. L.; Zhang, Y.; Ji, G.; Ma, L.; Chen, J. L.; Xu, B.; Tian, W. J. Multifunctional polymer nanoparticles, ultra bright near-infrared fluorescence and strong magnetization and their biological applications. *RSC Adv.* **2016**, *6*, 65426−65433.
2 Ji, G.; Yan, L. L.; Wang, H.; Ma, L.; Xu, B.; Tian, W. J. Efficient near-infrared AIE nanoparticles for cell imaging. *Acta Chimica Sinica* (in Chinese) **2016**, *74*, 917−922.
3 Zhang, F. L.; Di, Y. Z.; Li, Y.; Qi, Q. K.; Qian, J. Y.; Fu, X. Q.; Xu, B.; Tian, W. J. Highly efficient far red/near-infrared fluorophores with aggregation-induced emission for bioimaging. *Dyes Pigments* **2017**, *142*, 491−498.
4 Kobat, D.; Horton, N. G.; Xu, C. *In vivo* two-photon microscopy to 1.6-mm depth in mouse cortex. *J. Biomed. Opt.* **2011**, *16*, 106014.
5 Qian, J.; Wang, D.; Cai, F. H.; Zhan, Q. Q.; Wang, Y. L.; He, S. L. Photosensitizer encapsulated organically modified silica nanoparticles for direct two-photon photodynamic therapy and *in vivo* functional imaging. *Biomaterials* **2012**, *33*, 4851−4860.
6 Lakowicz, J. R. Plasmonics in biology and plasmon-controlled fluorescence. *Plasmonics* **2006**, *1*, 5−33.
7 Hinds, S.; Myrskog, S.; Levina, L.; Koleilat, G.; Yang, J.; Kelley, S. O.; Sargent, E. H. NIR-emitting colloidal quantum dots having 26% luminescence quantum yield in buffer solution. *J. Am. Chem. Soc.* **2007**, *129*, 7218−7219.
8 Yong, K. T.; Roy, I.; Ding, H.; Bergey, E. J.; Prasad, P. N. Biocompatible near-infrared quantum dots as ultrasensitive probes for long-term *in vivo* imaging applications. *Small* **2009**, *5*, 1997−2004.
9 Dabbousi, B. O.; Rodriguez-Viejo, J.; Mikulec, F. V.; Heine, J. R.; Mattoussi, H.; Ober, R.; Jensen, K. F.; Bawendi, M. G. (CdSe) ZnS core-shell quantum dots: Synthesis and characterization of a size series of highly luminescent nanocrystallites. *J. Phys. Chem. B* **1997**, *101*, 9463−9475.
10 Shi, L. J.; Zhu, C. N.; He, H.; Zhu, D. L.; Zhang, Z. L.; Pang, D. W.; Tian, Z. Q. Near-infrared Ag_2Se quantum dots with distinct absorption features and high fluorescence quantum yields. *RSC Adv.* **2016**, *6*, 38183−38186.
11 Wu, C. X.; Zhang, Y. J.; Li, Z.; Li, C. Y.; Wang, Q. B. A novel photoacoustic nanoprobe of ICG@PEG-Ag_2S for atherosclerosis targeting and imaging *in vivo*. *Nanoscale* **2016**, *8*, 12531−12539.
12 Han, H. J.; Wang, H. B.; Chen, Y. J.; Li, Z. H.; Wang, Y.; Jin, Q.; Ji, J. Theranostic reduction-sensitive gemcitabine prodrug micelles for near-infrared imaging and pancreatic cancer therapy. *Nanoscale* **2016**, *8*, 283−291.
13 Luo, S. L.; Zhang, E. L.; Su, Y. P.; Cheng, T. M.; Shi, C. M. A review of NIR dyes in cancer targeting and imaging. *Biomaterials* **2011**, *32*, 7127−7138.
14 Gao, X. H.; Yang, L. L.; Petros, J. A.; Marshal, F. F.; Simons, J. W.; Nie, S. M. *In vivo* molecular and cellular imaging with quantum dots. *Curr. Opin. Biotechnol.* **2005**, *16*, 63−72.
15 Escobedo, J. O.; Rusin, O.; Lim, S.; Strongin, R. M. NIR dyes for bioimaging applications. *Curr. Opin. Chem. Biol.* **2010**, *14*, 64−70.
16 Thomas, S. W.; Joly, G. D.; Swager, T. M. Chemical sensors based on amplifying fluorescent conjugated polymers. *Chem. Rev.* **2007**, *107*, 1339−1386.
17 Brasseur, N.; Nguyen, T. L.; Langlois, R.; Ouellet, R.; Marengo, S.; Houde, D.; van Lier, J. E. Synthesis and photodynamic activities of silicon 2,3-naphthalocyanine derivatives. *J. Med. Chem.* **1994**, *37*, 415−420.
18 Birks, J. B. in *Photophysics of aromatic molecules*, Wiley, London, UK, **1970**.
19 Tang, B. Z.; Zhan, X.; Yu, G.; Lee, P.; Liu, Y.; Zhu, D. B. Efficient blue emission from siloles. *J. Mater. Chem.* **2001**, *11*, 2974−2978.
20 Luo, J. D.; Xie, Z. L.; Lam, J. W. Y.; Cheng, L.; Chen, H. Y.; Qiu, C. F.; Kwok, H. S.; Zhan, X. W.; Liu, Y. Q.; Zhu, D. B.; Tang, B. Z. Aggregation-induced emission of 1-methyl-1,2,3,4,5-pentaphenylsilole. *Chem. Commun.* **2001**, 1740−1741.
21 Hong, Y. N.; Lam, J. W. Y.; Tang, B. Z. Aggregation-induced emission, phenomenon, mechanism and applications. *Chem. Commun.* **2009**, 4332−4353.
22 Mei, J.; Hong, Y. N.; Lam, J. W. Y.; Qin, A. J.; Tang, Y. H.; Tang, B. Z. Aggregation-induced emission: The whole is more brilliant than the parts. *Adv. Mater.* **2014**, *26*, 5429−5479.
23 Ding, D.; Li, K.; Liu, B.; Tang, B. Z. Bioprobes based on AIE fluorogens. *Acc. Chem. Res.* **2013**, *46*, 2441−2453.
24 Hong, Y. N.; Lam, J. W. Y.; Tang, B. Z. Aggregation-induced emission. *Chem. Soc. Rev.* **2011**, *40*, 5361−5388.
25 Mei, J.; Leung, N. L. C.; Kwok, R. T. K.; Lam, J. W. Y.; Tang, B. Z. Aggregation-induced emission: Together we shine, united we soar! *Chem. Rev.* **2015**, *115*, 11718−11940.
26 Zhang, X. Y.; Wang, K.; Liu, M. Y.; Zhang, X. Q.; Tao, L.; Chen, Y. W.; Wei, Y. Polymeric AIE-based nanoprobes for biomedical applications: Recent advances and perspectives. *Nanoscale* **2015**, *7*, 11486−11508.
27 Yan, L. L.; Zhang, Y.; Xu, B.; Tian, W. J. Fluorescent nanoparticles based on AIE fluorogens for bioimaging. *Nanoscale* **2016**, *8*, 2471−2487.
28 Zhang, Y.; Chen, Y. J.; Li, X.; Zhang, J. B.; Chen, J. L.; Xu, B.; Fu, X. Q.; Tian, W. J. Folic acid-functionalized AIE Pdots based on amphiphilic PCL-*b*-PEG for targeted cell imaging. *Polym. Chem.* **2014**, *5*, 3824−3830.
29 Zhang, X. Q.; Zhang, X. Y.; Wang, S. Q.; Liu, M. Y.; Tao, L.; Wei, Y. Surfactant modification of aggregation-induced emission material as biocompatible nanoparticles: Facile preparation and cell imaging. *Nanoscale* **2013**, *5*, 147−150.
30 Qin, W.; Ding, D.; Liu, J. Z.; Yuan, W. Z.; Hu, Y.; Liu, B.; Tang, B. Z. Biocompatible nanoparticles with aggregation-induced emission characteristics as far-red/near-infrared fluorescent bioprobes for *in vitro* and *in vivo* imaging applications. *Adv. Funct. Mater.* **2012**, *22*, 771−779.
31 Geng, J. L.; Li, K.; Ding, D.; Zhang, X. H.; Qin, W.; Liu, J. Z.; Tang, B. Z.; Liu, B. Lipid-PEG-folate encapsulated nanoparticles with aggregation induced emission characteristics: Cellular uptake mechanism and two-photon fluorescence ima-

ging. *Small* **2012**, *8*, 3655−3663.
32 Geng, J. L.; Li, K.; Pu, K. Y.; Ding, D.; Liu, B. Conjugated polymer and gold nanoparticle co-loaded PLGA nanocomposites with eccentric internal nanostructure for dual-modal targeted cellular imaging. *Small* **2013**, *9*, 2012−2019.
33 Li, K.; Qin, W.; Ding, D.; Tomczak, N.; Geng, J. L.; Liu, R. R.; Liu, J. Z.; Zhang, X. H.; Liu, H. W.; Liu, B.; Tang, B. Z. Photostable fluorescent organic dots with aggregation-induced emission (AIE dots) for noninvasive long-term cell tracing. *Sci. Rep.* **2013**, *3*, 1150.
34 Wang, Z. L.; Yan, L. L.; Zhang, L.; Chen, Y. J.; Li, H.; Zhang, J. B.; Zhang, Y.; Li, X.; Xu, B.; Fu, X. Q.; Sun, Z. C.; Tian, W. J. Ultra bright red AIE dots for cytoplasm and nuclear imaging. *Polym. Chem.* **2014**, *5*, 7013−7020.
35 Zhang, Y.; Chang, K. W.; Xu, B.; Chen, J. L.; Yan, L. L.; Ma, S. Q.; Wu, C. F.; Tian, W. J. Highly efficient near-infrared organic dots based on novel AEE fluorogen for specific cancer cell imaging. *RSC Adv.* **2015**, *5*, 36837−36844.
36 Wang, L.; Tan, W. H. Multicolor FRET silica nanoparticles by single wavelength excitation. *Nano Lett.* **2006**, *6*, 84−88.
37 Zhang, J.; Lakowicz, J. R. A model for DNA detection by metal-enhanced fluorescence from immobilized silver nanoparticles on solid substrate. *J. Phys. Chem. B* **2006**, *110*, 2387−2392.
38 Jin, Y. H.; Ye, F. M.; Zeigler, M.; Wu, C. F.; Chiu, D. T. Near-infrared fluorescent dye-doped semiconducting polymer dots. *ACS Nano* **2011**, *5*, 1468−1475.
39 Chung, C. Y. S.; Yam, V. W. W. Selective label-free detection of G-quadruplex structure of human telomere by emission spectral changes in visible-and-NIR region under physiological condition through the FRET of a two-component PPE-SO_3^--Pt(II) complex ensemble with Pt···Pt, electrostatic and π-π interactions. *Chem. Sci.* **2013**, *4*, 377−387.
40 Zhang, X. J.; Yu, J. B.; Rong, Y.; Ye, F. M.; Chiu, D. T.; Uvdal, K. High-intensity near-IR fluorescence in semiconducting polymer dots achieved by cascade FRET strategy. *Chem. Sci.* **2013**, *4*, 2143−2151.
41 Wagh, A.; Qian, S. Y.; Law, B. Development of biocompatible polymeric nanoparticles for *in vivo* NIR and FRET imaging. *Bioconjugate Chem.* **2012**, *23*, 981−992.
42 Geng, J. L.; Zhu, Z. S.; Qin, W.; Ma, L.; Hu, Y.; Gurzadyan, G. G.; Tang, B. Z.; Liu, B. Near-infrared fluorescence amplified organic nanoparticles with aggregation-induced emission characteristics for *in vivo* imaging. *Nanoscale* **2014**, *6*, 939−945.
43 Xie, Z. Q.; Yang, B.; Xie, W. J.; Liu, L. L.; Shen, F. Z.; Wang, H. A.; Yang, X. Y.; Wang, Z. M.; Li, Y. P.; Hanif, M.; Yang, G. D.; Ye, L.; Ma, Y. G. A class of nonplanar conjugated compounds with aggregation-induced emission, structural and optical properties of 2,5-diphenyl-1,4-distyrylbenzene derivatives with all *cis* double bonds. *J. Phys. Chem. B* **2006**, *110*, 20993−21000.
44 Hong, G. S.; Zou, Y. P.; Antaris, A. L.; Diao, S.; Wu, D.; Cheng, K.; Zhang, X. D.; Chen, C. X.; Liu, B.; He, Y. H.; Wu, J. Z.; Yuan, J.; Zhang, B.; Tao, Z. M.; Fukunaga, C.; Dai, H. J. Ultrafast fluorescence imaging *in vivo* with conjugated polymer fluorophores in the second near-infrared window. *Nat. Commun.* **2014**, *5*, 4206.
45 Rust, M. J.; Bates, M.; Zhuang, X. Sub-diffraction-limit imaging by stochastic optical reconstruction microscopy (STORM). *Nat. Methods* **2006**, *3*, 793−795.
46 Betzig, E.; Patterson, G. H.; Sougrat, R.; Lindwasser, O. W.; Olenych, S.; Bonifacino, J. S.; Davidson, M. W.; Lippincott-Schwartz, J.; Hess, H. F. Imaging intracellular fluorescent proteins at nanometer resolution. *Science* **2006**, *313*, 1642−1645.
47 Axelrod, D. Total internal reflection fluorescence microscopy in cell biology. *Traffic* **2001**, *2*, 764−774.
48 Chen, B.; Feng, G. X.; He, B. R.; Goh, C.; Xu, S. D.; Ramos-Ortiz, G.; Aparicio-Ixta, L.; Zhou, J.; Ng, L. G.; Zhao, Z. J.; Liu, B.; Tang, B. Z. Silole-based red fluorescent organic dots for bright two-photon fluorescence *in vitro* cell and *in vivo* blood vessel imaging. *Small* **2016**, *12*, 782−792.
49 Lou, X. D.; Zhao, Z. J.; Tang, B. Z. Organic dots based on AIEgens for two-photon fluorescence bioimaging. *Small* **2016**, *12*, 6430−6450.
50 Zhen, S. J.; Wang, S. W.; Li, S. W.; Luo, W. W.; Gao, M.; Ng, L. G.; Goh, C. C.; Qin, A. J.; Zhao, Z. J.; Liu, B.; Tang, B. Z. Efficient red/near-infrared fluorophores based on benzo[1,2-*b*:4,5-*b*']dithiophene 1,1,5,5-tetraoxide for targeted photodynamic therapy and *in vivo* two-photon fluorescence bioimaging. *Adv. Funct. Mater.* **2018**, *28*, 1706945.
51 Shen, X. Y.; Yuan, W. Z.; Liu, Y.; Zhao, Q. L.; Lu, P.; Ma, Y. G.; Williams, I. D.; Qin, A. J.; Sun, J. Z.; Tang, B. Z. Fumaronitrile-based fluorogen, red to near-infrared fluorescence, aggregation-induced emission, solvatochromism, and twisted intramolecular charge transfer. *J. Phys. Chem. C* **2012**, *116*, 10541−10547.
52 Liu, W.; Wang, Y. L; Han, X.; Lu, P.; Zhu, L.; Sun, C. W.; Qian, J.; He, S. L. Fluorescence resonance energy transfer (FRET) based nanoparticles composed of AIE luminogens and NIR dyes with enhanced three-photon near-infrared emission for *in vivo* brain angiography. *Nanoscale* **2018**, *10*, 10025−10032.
53 Wang, Y.; Hu, R.; Xi, W.; Cai, F.; Wang, S.; Zhu, Z.; Bai, R.; Qian, J. Red emissive AIE nanodots with high two-photon absorption efficiency at 1040 nm for deep-tissue *in vivo* imaging. *Biomed. Opt. Express* **2015**, *6*, 3783−3794.
54 Alifu, N.; Yan, L. L.; Zhang, H. Q.; Zebibula, A.; Zhu, Z. G.; Xi, W.; Roe, A. W.; Xu, B.; Tian, W. J.; Qian, J. Organic dye doped nanoparticles with NIR emission and biocompatibility for ultra-deep *in vivo* two-photon microscopy under 1040 nm femtosecond excitation. *Dyes Pigments* **2017**, *143*, 76−85.
55 Han, X.; Bai, Q.; Yao, L.; Liu, H. C.; Gao, Y.; Li, J. Y.; Liu, L. Q.; Liu, Y. L.; Li, X. X.; Lu, P.; Yang, B. Highly efficient solid-state near-infrared emitting material based on triphenylamine and diphenylfumaronitrile with an EQE of 2.58% in non-doped organic light-emitting diode. *Adv. Funct. Mater.* **2015**, *25*, 7521−7529.
56 Zhu, Z. F.; Qian, J.; Zhao, X. Y.; Qin, W.; Hu, R. R.; Zhang, H. Q.; Li, D. Y.; Xu, Z. P.; Tang, B. Z.; He, S. L. Stable and size-tunable aggregation-induced emission nanoparticles encapsulated with nanographene oxide and applications in three-photon fluorescence bioimaging. *ACS Nano* **2016**, *10*, 588−597.
57 Lakowicz, J. R. in *Principles of fluorescence spectroscopy*, Springer, Berlin, 3rd ed., **2006**.
58 Polavarapu, L.; Manna, M.; Xu, Q. H. Biocompatible glutathione capped gold clusters as one- and two-photon excitation fluorescence contrast agents for live cells imaging. *Nanoscale* **2011**, *3*, 429−434.

https://doi.org/10.1007/s10118-019-2206-3